Leaky-Wave Thinned Phased Array in PCB Technology for Telecommunication Applications

Blanco, D.; Rajo-Iglesias, E.; Montesano, A.; Llombart Juan, N.

DOI
10.1109/tap.2016.2597642

Publication date
2016

Document Version
Accepted author manuscript

Published in
IEEE Transactions on Antennas and Propagation

Leaky-Wave Thinned Phased Array in PCB Technology for Telecommunication Applications

Darwin Blanco, Eva Rajo-Iglesias, *Senior Member, IEEE*, Antonio Montesano Benito, and Nuria Llombart, *Senior Member, IEEE*

***Abstract*— We present a practical implementation of a leaky-wave thinned phased array in printed circuit board (PCB) technology. In this paper, we demonstrate that a reduction of the grating lobes, and therefore an improved gain in a thinned phased array, with respect to standard solutions, is achieved by virtue of the angular filtering introduced by a leaky-wave cavity in the far field. The presented array is designed in PCB and integrated with an inductive partial reflective surface. A full study of the performances of the 7 × 7 phased array antenna for several scanning angles and frequencies is presented. This paper shows an improved gain, directivity, grating lobe level, back lobe level, beam efficiency, and active reflection coefficient with respect to a reference solution based on 2 × 2 subarrays. The results are validated via the measurements of a 3 × 3 array prototype.**

***Index Terms*— Gain enhancement, leaky-wave antennas (LWAs), phased array, thinned array, TM_0 mode suppression.**

I. Introduction

EARTH and planetary coverage applications from geostationary orbit require high gain antennas over limited angular regions (typically a semiangle of 10°–15°). For these applications, it is possible to use large phased array antennas that can steer the beam over such limited coverage area [1]. For this application scenario, it is important to reduce the cost and complexity, which is directly related to the number of active transceivers required for the phased array antenna. Therefore, there is the interest to investigate the possibility of using thinned phased arrays with periods above a wavelength. This reduction in the number of array elements will introduce grating lobes in the visible range leading to a loss of efficiency. In order to reduce this efficiency loss, different approaches have been introduced in literature (see [2], [3] for a good overview of the state of the art). Most of the approaches use sparse array configurations with complex optimized array element positions and dimensions [4]–[7]. Optimizing positions and dimensions of the array elements suppresses grating lobes, but it does not avoid the average main-beam power loss with scan [8]. A different approach is to use periodic tight arrays where the phasing is done at subarray level [9]–[13]. This approach will attenuate the level of the grating lobes over a limited coverage region.

TABLE I
SPECIFICATIONS FOR THE APPLICATION SCENARIO

Scenario	
Pointing angle	$\Delta\theta = 8.6deg$
Inter-element distance	$2\lambda_0$
Work band (GHz)	Ku-band (14.25-14.5)
Elements distribution	7x7 Square lattice
Polarization	Linear

The suppression of the grating lobe in thinned phased arrays by means of a spatial dielectric filter or partially reflecting surface (PRS) was first proposed in [2]. Since then, the use of PRSs to enhance the directivity of small antennas has been considerably studied in literature [14]–[27]. This type of antennas is referred, in the literature, as leaky-wave antennas (LWAs) [17]–[19], electromagnetic bandgap (EBG) antennas [21], Fabry–Perot Antennas (FPAs) [22] and even resonant cavity antennas [25]. LWAs make use of a partially transmissive resonant structure [17] which can be made of a thin dielectric superstrate [17], [23], [24] or by using inductive- or capacitive-metasurfaces [18]–[22], [24], [25].

In [15], the guidelines for designing thinned phased arrays with a limited scanning angular range based on these leaky-wave cavities were described in terms of bandwidth and mutual coupling. It was concluded that the mutual coupling between two adjacent array elements had to be in the order of -20 dB to obtain the highest gain in the embedded pattern, similarly as in the case of focal plane arrays in the presence of PRS [26]. In [28], it was shown that an inductive strip grid-based PRS leads to higher directivity enhancement, in comparison with dielectric-based or capacitive-based PRS, but without compromising the antenna frequency bandwidth or mutual coupling as a result of the suppression of the TM_0 undesired leaky mode.

In this paper, we describe a practical implementation in printed circuit board (PCB) technology of the PRS-based thinned array concept. The PRS is optimized following the guidelines derived in [15] and [28] for maximum gain enhancement in the target scan coverage. This implementation

Manuscript received August 20, 2015; revised April 25, 2016; accepted July 21, 2016. Date of publication August 2, 2016; date of current version October 4, 2016. This work was supported in part by the Spanish Government under Project TEC2013-44019-R and in part by the Madrid Regional Government under Project S2013/ICE-3000.

D. Blanco was with the Department of Communications and Signal Theory, Carlos III de Madrid, 28911 Madrid, Spain. He is now with the Institute of Electronics and Telecommunications of Rennes, IETR, UMR CNRS 6164, University of Rennes 1, 35042 Rennes, France (e-mail: darwin.blanco-montero@univ-rennes1.fr).

E. Rajo-Iglesias is with the Department of Communications and Signal Theory, Carlos III University, 28911 Madrid, Spain (e-mail: eva@tsc.uc3m.es).

A. Montesano Benito is with Airbus Defense & Space, 28022 Madrid, Spain (e-mail: antonio.montesano@airbus.com).

N. Llombart is with the Terahertz Sensing Group, Delft University of Technology, 2628 CD Delft, The Netherlands (e-mail: n.llombartjuan@tudelft.nl).

Color versions of one or more of the figures in this paper are available online at http://ieeexplore.ieee.org.

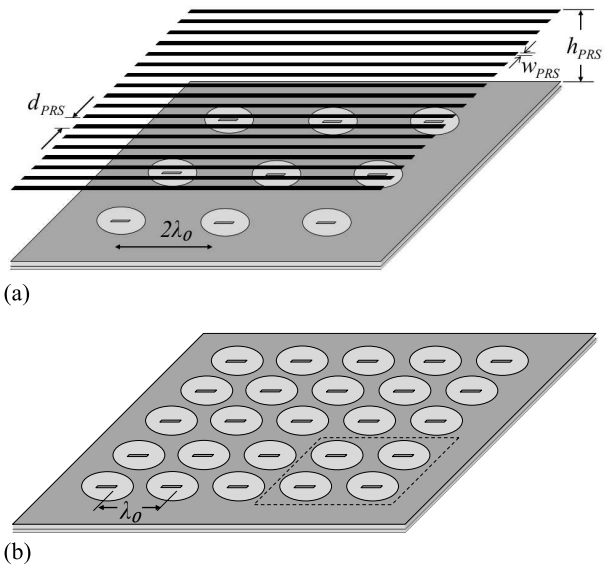

Fig. 1. (a) Leaky-wave thinned phased array: h_{PRS} is the cavity height, and d_{PRS} and w_{PRS} are the PRS periodicity and strip width, respectively. The array has a periodicity of $2\lambda_0$. (b) Thinned phased array composed by 2×2 subarrays. The array element spacing is λ_0, but the phase shifting is applied at the subarray level (i.e., corresponding to a periodicity of $2\lambda_0$).

fulfills the specifications, summarized in Table I, for future telecommunication Ku-band satellites.

The array phase-shifting is performed on array elements separated a distance of $2\lambda_0$ to reduce the front-end cost. Two array configurations, shown in Fig. 1(a) and (b), are designed in PCB technology and optimized to fulfill these requirements: an array of LWA elements and a more classical approach consisting of array elements made by 2×2 subarrays. The number of elements in the leaky-wave array is decimated by a factor of 4 with respect to the reference array. For this scenario, the grating lobes will appear in the angular region from 26° to 90° for the considered scanning range.

This paper is structured as follows. In section II, the optimization process in terms of the radiation pattern for designing the single array element is summarized. Section III presents the simulated performance for the two arrays with 7×7 elements. A complete study of the main parameters: gain (G), directivity (D), grating lobe level (GL), back lobe level (FB), and beam efficiency (BE) as a function of the frequency for the leaky-wave array compared to the reference array is reported also in this section. All numerical results of this paper have been calculated with CST MWS [29].

Finally, Section IV describes the manufactured prototypes and the experimental results.

II. Array Element Optimization

The geometry of the array element is shown in Fig. 2. The array is printed on a double grounded substrate of dielectric constant $\epsilon_r = 2.2$ and with a height of $h = 3.2$ mm. The height is selected in such a way that only the TM_0 surface wave inside this substrate is above cutoff. Surrounding the antenna, there is a circular cavity of radius $r_s = 9.15$ mm made of via-holes to avoid the propagation of this surface wave. The antenna is matched to a 50-Ω SubMiniature version

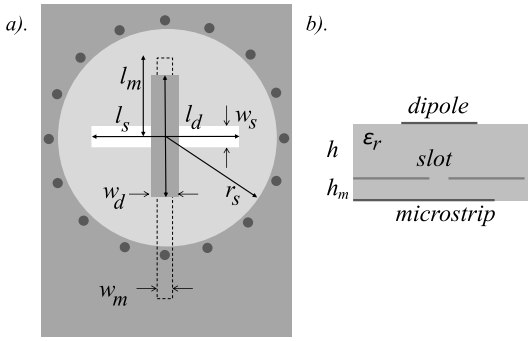

Fig. 2. Antenna geometry of the single element. Top and side views of the printed antenna microstrip element: slot (l_s; w_s) in a via-hole-based circular cavity (r_s) coupled to a dipole (l_d; w_d) and excited via microstrip (l_m; w_m). (a) Top view. (b) Side view.

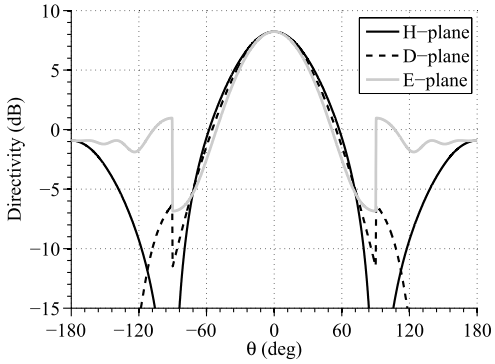

Fig. 3. Simulated radiation patterns of the array element designed in PCB (this element will be used for the two arrays). The observed discontinuity at 90° is due to the infinite ground plane that has been used in the simulation.

A (SMA) connector via a microstrip line and a stub with dimensions $l_m = 5.20$ mm (length of stub) and $w_m = 0.50$ mm (width of the stub). The dielectric substrate for the microstrip stub has a thickness of $h_m = 0.5$ mm and the same permittivity $\epsilon_r = 2.2$. The presented antenna is similar to the one reported in [30] where a planar EBG was used to suppress the TM_0 surface wave instead of the via-holes proposed in this configuration. At the bottom of the circular cavity, there is a slot excited via the mentioned microstrip line with the stub. The width and length of the slot are $w_s = 0.79$ mm and $l_s = 10.50$ mm, respectively. At the top of the cavity there is a dipole of length $l_d = 7.68$ mm and width $w_d = 0.20$ mm used to increase the frequency bandwidth of the antenna and to improve the symmetry of the radiated field in the main planes. The optimal solution was selected with respect to the symmetry of the pattern and the reflection coefficient. In Fig. 3, the radiated field of the proposed antenna element is shown, here the good rotational symmetry of the patterns is clearly observed.

This element geometry will be used as the building element in the reference array as well as in the leaky-wave one. For the proposed leaky-wave approach, an inductive PRS at certain height h_{PRS} as shown in Fig. 1(a) is located on top of the ground plane. Instead, the benchmark case is composed of a 2×2 subarray with the elements placed at a distance of λ_0 from each other [see Fig. 1(b)]. Following the conclusions derived in [15] and [28], we have designed the PRS ($d_{\mathrm{PRS}} = 5.20$ mm, $w_{\mathrm{PRS}} = 1.05$ mm, and

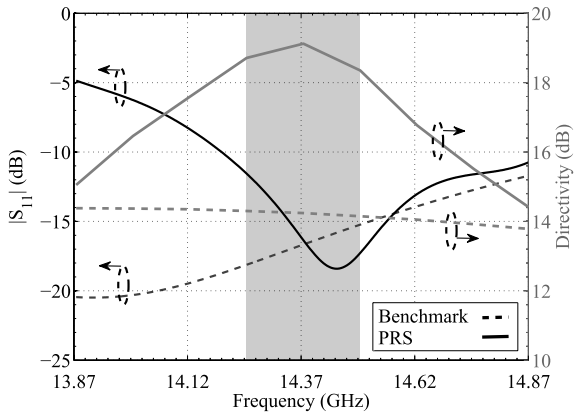

Fig. 4. Magnitude of the reflection coefficient S_{11} and directivity for PRS leaky-wave element (solid lines) compared with the basic printed antenna element (2×2 subarray) of the benchmark reference (dashed lines). The magnitude of the reflection coefficient is shown in the left axis, whilst the directivity is represented in the right one.

$h_{\text{PRS}} = 9.55$ mm) in order to have a level of mutual coupling between the array elements at a distance of $2\lambda_0$ of -20 dB. The frequency selective surface (FSS) prototype has been designed to be equivalent to a dielectric superlayer structure with permittivity $\epsilon_r = 10$ in the resonant condition. The design frequency is 14.375 GHz. Fig. 4 shows the magnitude of the reflection coefficient S_{11} for both array elements. The benchmark one presents a very good matching over a frequency band of 25%. The PRS one, instead, presents a smaller bandwidth due to the resonant frequency behavior of the LWAs. Even so, this bandwidth is sufficient for the considered application (i.e., 14.25–14.50 GHz).

Fig. 4 also presents the directivity of the two designed array elements as a function of the frequency. Due to its resonant behavior, the directivity varies rapidly with the frequency in the PRS case. Nevertheless, the directivity for the PRS is larger than for the benchmark in the frequency bandwidth of interest. This directivity enhancement is linked to the use of a larger aperture size compared to the reference benchmark. The cross-polarization of the leaky-wave-based antenna in the upper half-space is negligible. Indeed, as described in [31], the broadside radiation generated by FPAs comes from almost perfectly polarized aperture field.

A 2-D representation of the farfield in elevation and azimuth at 14.375 GHz is shown in Figs. 5 and 6 for the benchmark and PRS array elements, respectively. The plots shown in Figs. 5(a) and (b) and 6(a) and (b) are the radiated fields in the upper half-space (i.e., $0° \leq \theta \leq 90°$). Instead, the plots shown in Figs. 5(c) and (d) and 6(c) and (d) are the radiated fields in the lower half-space (i.e., $90° \leq \theta \leq 180°$). Also in the left part of each figure we can find the copolarized fields whilst in the right side we have the cross-polarized fields. As we can see, the PRS antenna provides significant lower levels of cross polar component of the field than the benchmark as well as lower back lobe level. Fig. 7 shows the radiated fields for both antenna elements in the H-plane at 14.375 GHz as an example. We can appreciate that the PRS provides higher directivity, as a consequence of the leaky-wave enhancement and the lower back lobe level. In the same figure, the embedded pattern for the PRS case of the center element

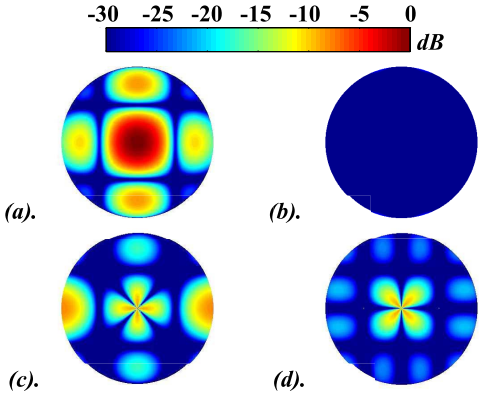

Fig. 5. 2-D representation of the benchmark array element radiation pattern. (a) Copolarized and (b) cross-polarized fields in the upper half-space. (c) Copolarized and (d) cross-polarized fields in the lower half-space.

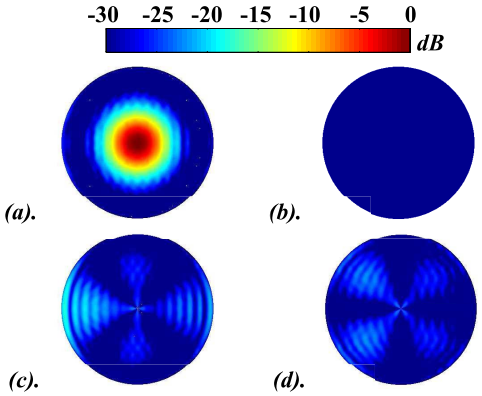

Fig. 6. 2-D representation of the PRS array element radiation pattern. (a) Copolarized and (b) cross-polarized fields in the upper half-space. (c) Copolarized and (d) cross-polarized fields in the lower half-space.

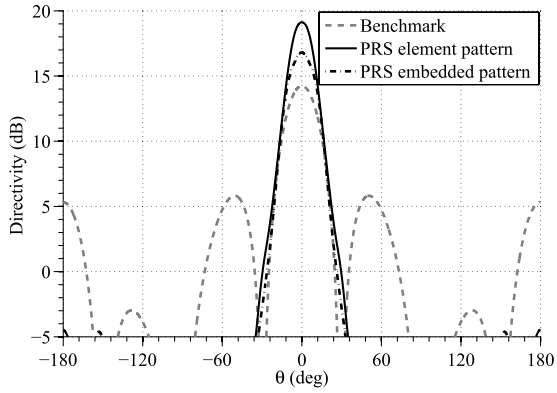

Fig. 7. H-plane radiation pattern of the benchmark and PRS-based array elements at the central frequencies (including embedded pattern for the PRS case using 5×5 elements).

in a 5×5 array configuration is also included. This element embedded pattern presents lower directivity due to the effect of the mutual coupling as described in [15] and [26]. Even if the directivity is reduced from the isolated case, the PRS case still leads to a larger attenuation of the grating lobes when compared to the benchmark case.

III. Phased Array Performances

The leaky thinned array has 7×7 elements spaced by $2\lambda_0$. Instead the benchmark based on subarrays has 14×14 elements separated by λ_0.

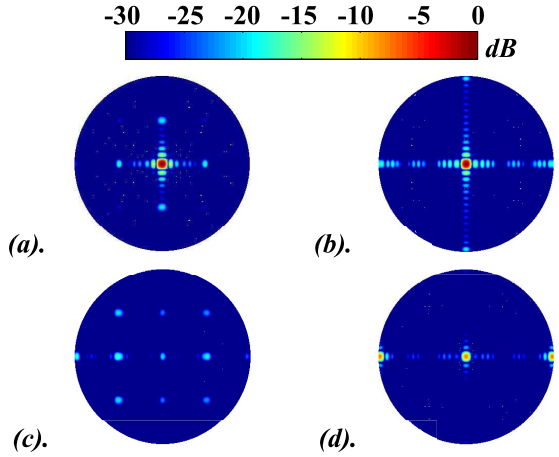

Fig. 8. Farfield in (a) and (b) upper and (c) and (d) lower half-space in a polar coordinate system of (a)–(c) 7×7 PRS and (b)–(d) benchmark arrays radiating at broadside.

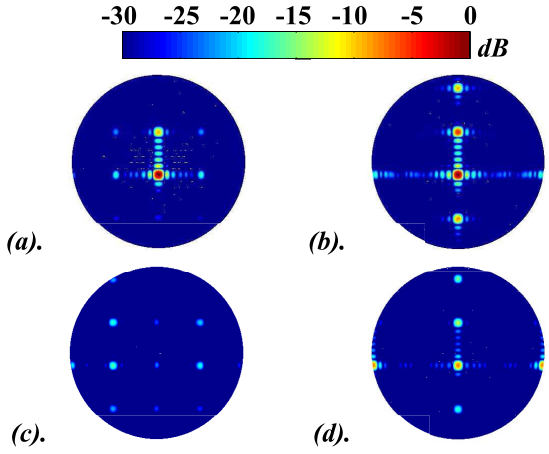

Fig. 9. Farfield in (a) and (b) upper and (c) and (d) lower half-space in a polar coordinate system of (a)–(c) 7×7 PRS and (b)–(d) benchmark arrays radiating at the scanning angle $\theta = 8.6°$ in the E-plane.

We present full wave simulations carried out with CST MWS [29] of 7×7 phased arrays scanning at broadside and at the edge of the scanning range, $\theta = 8.6°$, in both H- and E-planes. The array element phasing is made considering a spacing of $2\lambda_0$ for both cases.

One important parameter for the leaky-wave-based array is related to the dimensions of the ground plane and PRS. As it was mentioned in Section II, the LWA uses a significantly larger aperture compared to the 2×2 benchmark. For the array scenario, the difference in aperture dimensions between the two solutions is smaller, since only the edge elements need some extra area. The ground plane and PRS dimension should be long enough to have the leaky wave sufficiently attenuated, but not extremely large for practical reasons. In the simulations, the area of the leaky-wave array (i.e., ground plane and PRS) has been fixed to 20λ in order not to have an impact from the finite structure. Instead, a length of $L = 15\lambda$ leads to a small reduction of 0.2 dB of directivity, whereas a length of $L = 14\lambda$ (equivalent to the benchmark array) leads to a loss of 0.9 dB of directivity (at the central frequency with respect to $L = 20\lambda$).

A 2-D representation of the farfield in elevation and azimuth at the central frequency (i.e., 14.375 GHz), is shown in Figs. 8 and 9 for two of the three simulated scanning conditions. The plots shown in Figs. 8(a) and (b) and 9(a) and (b) are the radiated fields in the upper half-space for the PRS and benchmark arrays, respectively. Instead, the plots shown in Figs. 8(c) and (d) and 9(c) and (d) are the radiated fields in the lower half-space. As we can see, the PRS-based array provides higher attenuation of the grating lobes than the benchmark in all the cases. It is important to mention that for the benchmark case there is a significant loss of power in the backradiation (lower half-space), specially in the H-plane for the broadside condition (see Fig. 8). This effect reduces the value of the directivity in the upper half-space.

The simulated active reflection coefficients for all the 49 array elements at several scanning conditions have been calculated in CST and omitted in this section for brevity (we present all the s_{1j} coefficients in the experimental validation section). For all cases (in the benchmark and PRS), the active reflection coefficients are well-matched over the frequency band of interest. The bandwidth of the benchmark is obviously larger due to the inherent lower mutual coupling.

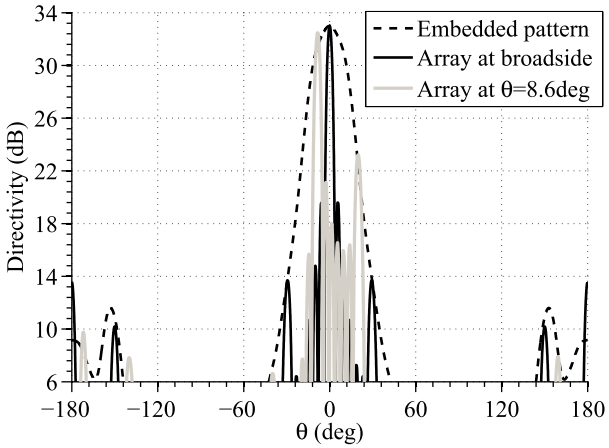

Fig. 10. H-plane radiation pattern at central frequency (14.375 GHz) for the 7×7 PRS array at broadside (dark solid line) and at scanning angle of $\theta = 8.6°$ (gray solid line) including also the 5×5 embedded pattern (dashed line).

Figs. 10 and 11 show the embedded and the array radiation pattern for two scanning conditions (at broadside and at scan angle of $\theta = 8.6°$) of both arrays in the H-plane at the central frequency. Due to the low level of mutual coupling (-20 dB), only the adjacent elements (at $2\lambda_0$) contribute to the embedded pattern. This means that we can calculate the embedded pattern from the central element of a 5×5 array or even 3×3 array without significant differences. In the benchmark case, the element pattern of the 2×2 subarray embedded in an array is basically the same than the isolated subarray, because this antenna presents a very low mutual coupling.

The position of the nearest grating lobe for the benchmark at broadside and at the maximum scanning angle is $\pm 90°$ (i.e., because the interelement distance at broadside in the subarray is λ_0) and $\pm 20°$, respectively. For the same situations, the grating lobes are at $\pm 30°$ and $\pm 20°$ for the PRS array. At broadside, the nearest grating lobe is

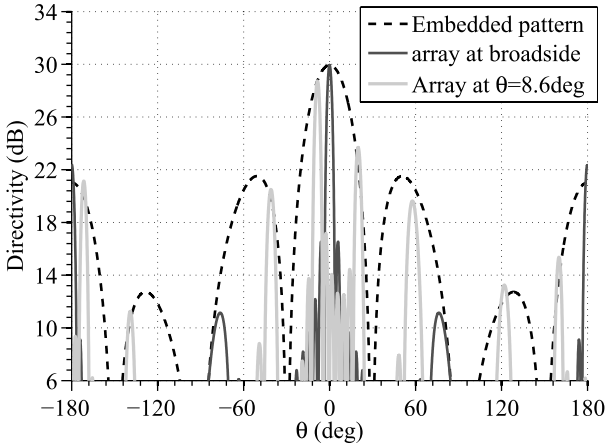

Fig. 11. H-plane radiation pattern at central frequency (14.375 GHz) for the 7×7 benchmark array at broadside (dark solid line) and at scanning angle of $\theta = 8.6°$ (gray solid line) including also the element pattern (dashed line).

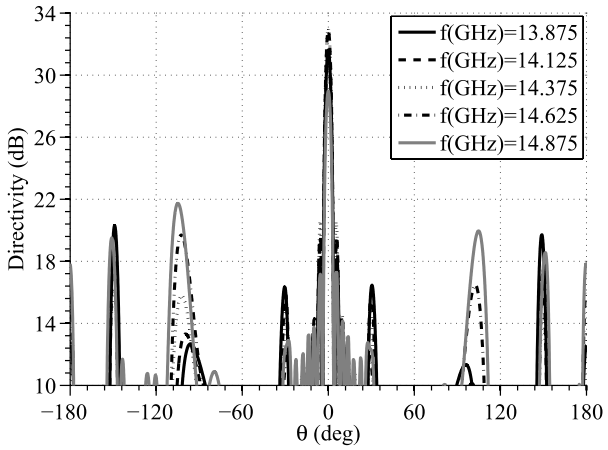

Fig. 12. E-plane radiation pattern for the 7×7 PRS array at broadside as a function of the frequency.

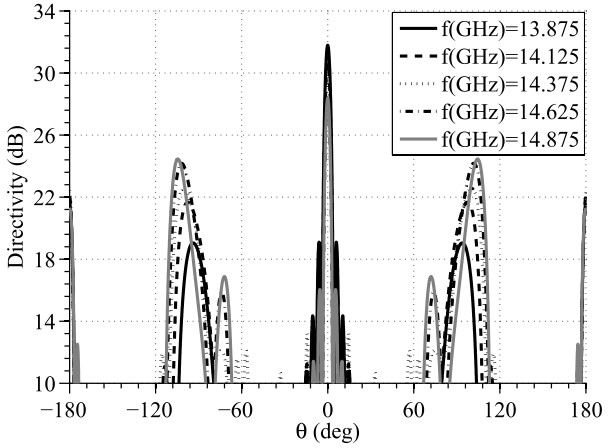

Fig. 13. E-plane radiation pattern for the 7×7 benchmark array at broadside as a function of the frequency.

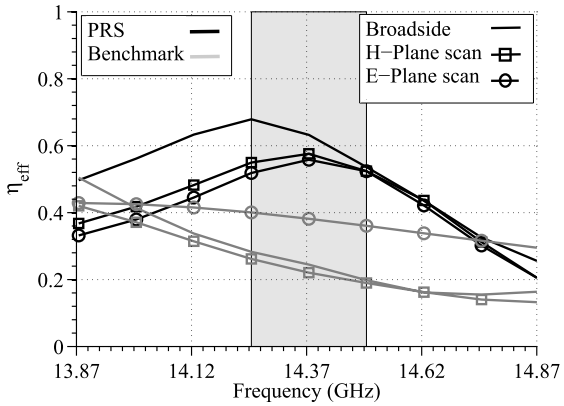

Fig. 14. Beam efficiency as a function of the frequency (at broadside and at the maximum scanning angle of $\theta = 8.6°$ in the H- and E-planes). Dark line: PRS array design. Gray line: reference benchmark array antenna. Solid-line: beam efficiency at broadside. Square-line: scan in the H-plane. Circle-line: scan in the E-plane.

attenuated 18.79 dB (benchmark) and 19.31 dB (PRS). A larger improvement in the suppression of the grating lobe can be clearly appreciated at the maximum scanning angle ($\theta = 8.6°$) as a result of the angular filtering of the PRS case respect to the benchmark. There, the benchmark only leads to a 5-dB attenuation of the grating lobe (i.e., attenuation respect to the maximum directivity at this scanning angle) whilst the PRS leads to 9.26 dB of attenuation.

Figs. 12 and 13 show the variation of the radiation pattern with the frequency for the E-plane at broadside for the 7×7 PRS and benchmark array, respectively. A reduction of the directivity as a function of the frequency can be observed for the 7×7 benchmark. This reduction is due to the higher level of back radiation. In contrast, the proposed 7×7 PRS array presents improved directivity in the entire frequency band.

In Fig. 14, the beam efficiency has been calculated for the 7×7 PRS array antenna and compared to the benchmark array at several scanning angles (at broadside and at the maximum scanning angle in the H- and E-planes). The beam efficiency is calculated as a function of the frequency by integrating the radiation intensity over the main beam with respect to the overall angular integral. In Fig. 14, the band of interest is also highlighted in gray. Observing Fig. 14, we can conclude that the PRS array presents a better beam efficiency in the band of interest (gray area) with respect to the reference benchmark composed of subarrays.

To finalize the performance analysis of the phased array, we present the variation of the main parameters as a function of the frequency for both the PRS-based and benchmark arrays at the three scanning conditions previously studied. We make the study of the frequency variation, for both arrays, of the simulated directivity (D), the gain (G), the grating lobe level (GL) and the back lobe level (FB). The grating lobe level has been calculated as the negative difference in decibel between the higher value of directivity and the higher value of the grating lobe [the angle for this value is nearby to the theoretical value of the grating lobe angle for scanning according to $\theta_{\mathrm{GL}} = \sin^{-1}(\lambda/d + \sin(\theta_{\mathrm{scan}}))$, where d represents the period]. Both values are calculated in the upper half-space. On other hand, the back lobe level (FB) is the negative difference in decibel between the higher value in the upper half-space and the higher value in the lower half-space. In both calculations, a more negative value represents

TABLE II

MAIN PARAMETERS OF THE 7 × 7 PHASED ARRAY COMPARED WITH THE REFERENCE BENCHMARK FOR THE THREE SCANNING ANGLES AT CENTRAL FREQUENCY. *D* REPRESENTS DIRECTIVITY, *G* GAIN, GL GRATING LOBE, SL SIDE LOBE, AND FB BACK LOBE LEVEL

Parameter	Broadside		H-plane		E-plane	
	Bench	PRS	Bench	PRS	Bench	PRS
D (dB)	29.94	33.01	28.73	32.48	30.87	32.5
G (dB)	29.91	32.92	28.69	32.35	30.67	32.4
GL (dB)	-7.36	-17.63	-5.04	-9.26	-7.16	-8.91
SL (dB)	-13.4	-12.4	-11.56	-11.36	-11.96	-11.24
FB (dB)	-7.36	-16.79	-7.52	-16.41	-8.36	-17.29

better performance for the associated parameter. At broadside in the case of the benchmark, the location of the grating lobe is at 90° because as mentioned before, the interelement distance in the subarray is λ_0 and they are all-in-phase for broadside radiation. For this situation, the back lobe level is comparable to the grating lobe level. For the benchmark case, the radiation pattern when scanning in E-plane presents higher values of directivity than the same array in the other two studied situation (broadside and scanning in H plane) as a result of the lower values of backradiation as it can be clearly seen in Table II. These values of backradiation impact directly on the beam efficiency and would be one of the advantages of the PRS-based array. The PRS array provides larger directivity, and both lower grating lobe and back lobe levels (at broadside and also in the other two extreme scanning conditions). Over the frequency band specified in the application scenario (i.e., 14.25–14.50 GHz) and for the three scanning cases analyzed, the PRS array always provides at least 1.73 dB more gain than the benchmark array.

To summarize these results, Table II presents the directivity, gain, grating lobe level, side lobe level, and back lobe level at the central frequency. The increase in the PRS gain is associated to several facts: the reduction of the grating lobe and of the back radiation, and also a slight increase in the radiating area at the array edges [see Fig. 1(a)].

IV. EXPERIMENTAL VALIDATION

We have fabricated and measured two prototypes, referred to the isolated element and a 3 × 3 PRS phased array. The size of the ground plane and the PRS has been fixed for both prototypes to $10\lambda_0$ (by manufacturing facilities). The PRS is manufactured by photo-printing in a Kapton layer and also a supporting foam layer has to be added to the previous design. This Kapton (with 0.05 mm thickness and $\epsilon_r = 3$) is a flexible material that is laying in the thin foam layer (with 3 mm thickness and $\epsilon_r = 1.067$). With this new materials, the parameters of the FSS and their cavity must be recalculated as in [28]. The height of the cavity is now fixed to 6.44 mm and the width of the strip is 1.052 mm. The period of the FSS is kept as 5.2 mm.

The two prototypes have been manufactured with the dimensions described previously. Fig. 15 includes a picture of the 3 × 3 phased array. We have limited the number of elements in the array (from 7 × 7 to 3 × 3) due to manufacturing constrains and assuming that as the mutual coupling is low,

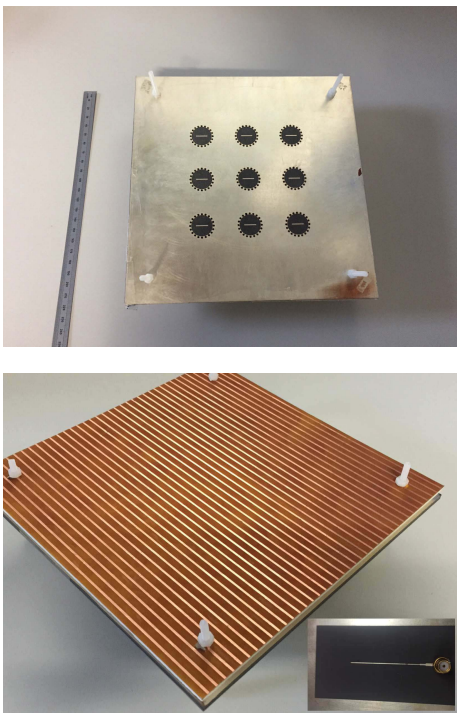

(a)

(b)

Fig. 15. (a) Manufactured 3 × 3 array. (b) Manufactured FSS. Inset: detailed photo of one of the vertical SMA connectors and the feeding microstrip line.

the 3 × 3 embedded element is enough representative of the real scenario. The measured S_{11} for the embedded element is shown in Fig. 16. In the same graph, the results from full wave simulations (for the isolated and embedded element) are included for comparison purposes.

The agreement is quite satisfactory, except for a small frequency shift for the S_{11} in the embedded measured prototype. This may be attributed to manufacturing tolerances of the PRS (made with basic photo-printing technique) and even the characterization of the Kapton itself. Besides the foam is not a rigid material and can therefore create tilts in the PRS. The higher level of the reflection coefficient that is also observed in Fig. 16, can be attributed to little displacements in the feeding layer. That layer is very thin and flexible and has been manually fixed with screws. A more accurate fabrication process would resolve both the shift in frequency and the higher level of the reflection coefficient.

As it was already reported in [27] and [28], the most critical parameters for the manufacturing process are associated with the Fabry–Perot cavity because it is highly resonant. For example, a variation of the 3% in the height of the cavity (+0.29 mm) could represent a frequency shift of 17.4% for the single element antenna. On the other hand, an inclination of around 1° in the PRS with respect to the ground plane can produce a loss in the magnitude of the reflection coefficient of around 5 dB.

The magnitude of the simulated and measured S_{i1} for the all ports in the 3 × 3 phased array is shown in Fig. 17. Because of the structure symmetries, only three different coefficients are shown. The agreement is satisfactory in all cases, the lower levels of the S_{i1} correspond with the higher levels of the measured S_{11} and the most important fact is that for both

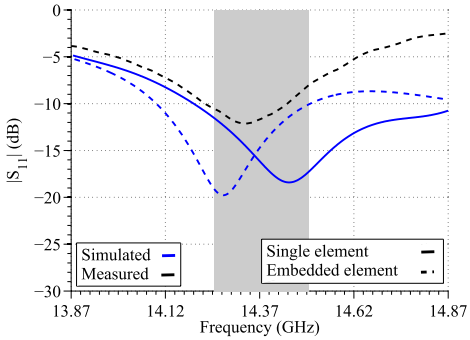

Fig. 16. Measured magnitude of reflection coefficient S_{11} for the embedded element and comparison with simulation results.

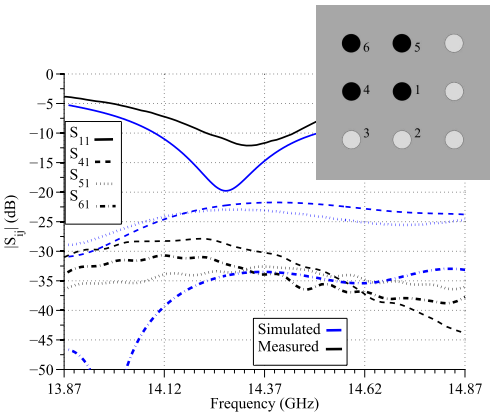

Fig. 17. Measured magnitude of the S_{ij} and comparison with simulation results. Inset: relative position of the surrounding elements.

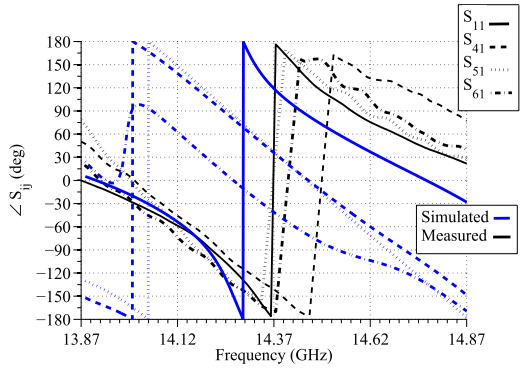

Fig. 18. Measured phase of the S_{ij} and comparison with simulation results.

the simulated and measured S_{i1}, i.e., the mutual coupling is always below the -20-dB level. Fig. 18 represents the measured phase of the S_{ij} parameters at broadside for the main H and E planes. The results of the full wave simulations for the active reflection coefficients are also shown for comparison purposes. These main differences in the measured phase of the S_{ij} parameters with respect to the simulated results can be attributed to the manufacturing process, in particular to the possible displacements in the feeding layer and/or little tilts in the vertical axes of the mini SMA connectors.

Finally, Fig. 19 includes for comparison the simulated results and the measured radiation patterns for the

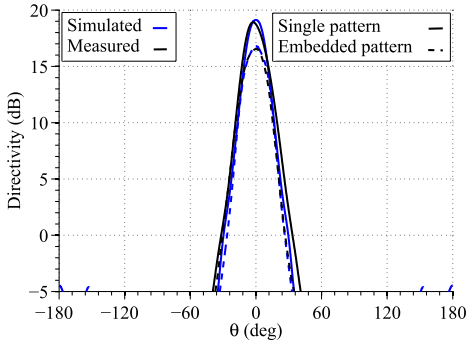

Fig. 19. Measured radiation pattern in H-plane for both the single element and the embedded element and comparison with simulation results.

two prototypes in the H-plane. Same agreement can be obtained for the E-plane but we omitted these results for brevity. As it can be seen, the measured radiation patterns agree quite well with the simulated ones.

V. Conclusion

This paper presents the design and implementation of a leaky-wave thinned phased array in PCB technology. The simulations and experimental results show that a reduction of the grating lobes and a consequent improved gain of the thinned array radiation pattern are possible by virtue of the angular filtering introduced by a Fabry–Perot/leaky-wave cavity.

The designed leaky-wave thinned phased array has been compared with a benchmark, based on phasing subarrays, that represents the current baseline in the telecom industry. A complete study of the directivity, gain, grating lobe level, and back lobe level as a function of frequency has been done. This paper shows an improved gain of about 1.73 dB for the leaky-wave thinned phased array in the entire band of interest and for all specified scanning angles. Measurements of a 3×3 prototype have confirmed the simulations.

The main drawback of the leaky-wave approach is the limitation in bandwidth, which is directly related to the required directivity enhancement and therefore the array spacing. The presented design is indeed extremely resonant with a bandwidth in the order of 3.5% because the required array spacing was $2\lambda_0$. In previous works [15], it has been demonstrated a comparable enhancement with smaller spacings ($1.5\lambda_0$) and larger bandwidths (10%).

References

[1] C. K. Ng, *Phased Array Antenna Beam Steering for Satellite Tracking*. Saarbrücken, Germany: Lambert Academic Publishing, 2009.

[2] R. Mailloux, L. Zahn, A. Martinez, III, and G. R. Forbes, "Grating lobe control in limited scan arrays," *IEEE Trans. Antennas Propag.*, vol. 27, no. 1, pp. 79–85, Jan. 1979.

[3] G. Toso and R. Mailloux, "Guest editorial for the special issue on innovative phased array antennas based on non-regular lattices and overlapped subarrays," *IEEE Trans. Antennas Propag.*, vol. 62, no. 4, pp. 1546–1548, Apr. 2014.

[4] P. Angeletti and G. Toso, "Array antennas with jointly optimized elements positions and dimensions part I: Linear arrays," *IEEE Trans. Antennas Propag.*, vol. 62, no. 4, pp. 1619–1626, Apr. 2014.

[5] A. Ishimaru, "Unequally spaced arrays based on the Poisson sum formula," *IEEE Trans. Antennas Propag.*, vol. 62, no. 4, pp. 1549–1554, Apr. 2014.
[6] B. Lu, S. X. Gong, S. Zhang, Y. Guan, and J. Ling, "Optimum spatial arrangement of array elements for suppression of grating-lobes of radar cross section," *IEEE Antennas Wireless Propag. Lett.*, vol. 9, pp. 114–117, 2010.
[7] M. G. Bray, D. H. Werner, D. W. Boeringer, and D. W. Machuga, "Optimization of thinned aperiodic linear phased arrays using genetic algorithms to reduce grating lobes during scanning," *IEEE Trans. Antennas Propag.*, vol. 50, no. 12, pp. 1732–1742, Dec. 2002.
[8] R. Mailloux and G. Forbes, "An array technique with grating-lobe suppression for limited-scan applications," *IEEE Trans. Antennas Propag.*, vol. 21, no. 5, pp. 597–602, Sep. 1973.
[9] V. D. Agrawal, "Grating-lobe suppression in phased arrays by subarray rotation," *Proc. IEEE*, vol. 66, no. 3, pp. 347–349, Mar. 1978.
[10] T. Sehm, A. Lehto, and A. V. Raisanen, "A high-gain 58-GHz box-horn array antenna with suppressed grating lobes," *IEEE Trans. Antennas Propag.*, vol. 47, no. 7, pp. 1125–1130, Jul. 1999.
[11] P. Angeletti, "Multiple beams from planar arrays," *IEEE Trans. Antennas Propag.*, vol. 62, no. 4, pp. 1750–1761, Apr. 2014.
[12] S. P. Skobelev, "On the forming of orthogonal beams by planar array antennas," *IEEE Trans. Antennas Propag.*, vol. 62, no. 4, pp. 1762–1768, Apr. 2014.
[13] D. Petrolati, P. Angeletti, and G. Toso, "A lossless beam-forming network for linear arrays based on overlapped sub-arrays," *IEEE Trans. Antennas Propag.*, vol. 62, no. 4, pp. 1769–1778, Apr. 2014.
[14] R. Gardelli, M. Albani, and F. Capolino, "Array thinning by using antennas in a Fabry–Perot cavity for gain enhancement," *IEEE Trans. Antennas Propag.*, vol. 54, no. 7, pp. 1979–1990, Jul. 2006.
[15] D. Blanco, N. Llombart, and E. Rajo-Iglesias, "On the use of leaky wave phased arrays for the reduction of the grating lobe level," *IEEE Trans. Antennas Propag.*, vol. 62, no. 4, pp. 1789–1795, Apr. 2014.
[16] G. V. Trentini, "Partially reflecting sheet arrays," *IRE Trans. Antennas Propag.*, vol. 4, no. 4, pp. 666–671, Oct. 1956.
[17] D. R. Jackson, A. A. Oliner, and A. Ip, "Leaky-wave propagation and radiation for a narrow-beam multiple-layer dielectric structure," *IEEE Trans. Antennas Propag.*, vol. 41, no. 3, pp. 344–348, Mar. 1993.
[18] T. Zhao, D. R. Jackson, J. T. Williams, H.-Y. D. Yang, and A. A. Oliner, "2-D periodic leaky-wave antennas—Part I: Metal patch design," *IEEE Trans. Antennas Propag.*, vol. 53, no. 11, pp. 3505–3514, Nov. 2005.
[19] T. Zhao, D. R. Jackson, and J. T. Williams, "2-D periodic leaky-wave antennas—Part II: Slot design," *IEEE Trans. Antennas Propag.*, vol. 53, no. 11, pp. 3515–3524, Nov. 2005.
[20] A. P. Feresidis, G. Goussetis, S. Wang, and J. C. Vardaxoglou, "Artificial magnetic conductor surfaces and their application to low-profile high-gain planar antennas," *IEEE Trans. Antennas Propag.*, vol. 53, no. 1, pp. 209–215, Jan. 2005.
[21] Y. J. Lee, J. Yeo, R. Mittra, and W. S. Park, "Application of electromagnetic bandgap (EBG) superstrates with controllable defects for a class of patch antennas as spatial angular filters," *IEEE Trans. Antennas Propag.*, vol. 53, no. 1, pp. 224–235, Jan. 2005.
[22] N. Guerin, S. Enoch, G. Tayeb, P. Sabouroux, P. Vincent, and H. Legay, "A metallic Fabry–Perot directive antenna," *IEEE Trans. Antennas Propag.*, vol. 54, no. 1, pp. 220–224, Jan. 2006.
[23] A. Neto and N. Llombart, "Wideband localization of the dominant leaky wave poles in dielectric covered antennas," *IEEE Antennas Wireless Propag. Lett.*, vol. 5, no. 1, pp. 549–551, Dec. 2006.
[24] G. Lovat, P. Burghignoli, and D. R. Jackson, "Fundamental properties and optimization of broadside radiation from uniform leaky-wave antennas," *IEEE Trans. Antennas Propag.*, vol. 54, no. 5, pp. 1442–1452, May 2006.
[25] A. Foroozesh and L. Shafai, "Investigation into the effects of the patch-type FSS superstrate on the high-gain cavity resonance antenna design," *IEEE Trans. Antennas Propag.*, vol. 58, no. 2, pp. 258–270, Feb. 2010.
[26] N. Llombart, A. Neto, G. Gerini, M. Bonnedal, and P. De Maagt, "Impact of mutual coupling in leaky wave enhanced imaging arrays," *IEEE Trans. Antennas Propag.*, vol. 56, no. 4, pp. 1201–1206, Apr. 2008.
[27] A. Neto, M. Ettorre, G. Gerini, and P. De Maagt, "Leaky wave enhanced feeds for multibeam reflectors to be used for telecom satellite based links," *IEEE Trans. Antennas Propag.*, vol. 60, no. 1, pp. 110–120, Jan. 2012.
[28] D. Blanco, E. Rajo-Iglesias, S. Maci, and N. Llombart, "Directivity enhancement and spurious radiation suppression in leaky-wave antennas using inductive grid metasurfaces," *IEEE Trans. Antennas Propag.*, vol. 63, no. 3, pp. 891–900, Mar. 2015.
[29] Spatial Corp. (Sep. 29, 2012). *CST Microwave Studio, Release Version 2012.06*. [Online]. Available: http://www.cst.com
[30] N. Llombart, A. Neto, G. Gerini, and P. De Maagt, "Planar circularly symmetric EBG structures for reducing surface waves in printed antennas," *IEEE Trans. Antennas Propag.*, vol. 53, no. 10, pp. 3210–3218, Oct. 2005.
[31] A. Polemi and S. Maci, "On the polarization properties of a dielectric leaky wave antenna," *IEEE Antennas Wireless Propag. Lett.*, vol. 5, no. 1, pp. 306–310, Dec. 2006.

Darwin Blanco received the Electrical Engineering degree from the University of Antioquia, Medellín, Colombia, in 2009, and the M.Sc. and Ph.D. (*summa cum laude*) degrees in multimedia and communications from the University Carlos III de Madrid, Madrid, Spain, in 2011 and 2014, respectively. He is currently pursuing the Ph.D. degree with the University of Rennes 1, Rennes, France.

His current research interests include leaky wave antennas and metasurfaces to be used in applications for phase array antennas, polarizers, and filters.

Eva Rajo-Iglesias (SM'08) was born in Monforte de Lemos, Spain, in 1972. She received the M.Sc. degree in telecommunication engineering from the University of Vigo, Vigo, Spain, in 1996, and the Ph.D. degree in telecommunication engineering from the University Carlos III of Madrid, Madrid, Spain, in 2002.

She was a Teaching Assistant with the University Carlos III of Madrid from 1997 to 2001. She joined the Polytechnic University of Cartagena, Cartagena, Spain, as a Teaching Assistant, in 2001. She joined the University Carlos III of Madrid as a Visiting Lecturer in 2002, where she has been an Associate Professor with the Department of Signal Theory and Communications since 2004. She visited the Chalmers University of Technology, Gothenburg, Sweden, as a Guest Researcher, from 2004 to 2008, where she has been an Affiliate Professor with the Antenna Group, Signals and Systems Department, since 2009. She has co-authored more than 50 papers in JCR international journals and more than 100 papers in international conferences. Her current research interests include microstrip patch antennas and arrays, metamaterials, artificial surfaces and periodic structures, gap waveguide technology, MIMO systems, and optimization methods applied to electromagnetism.

Dr. Rajo-Iglesias was a recipient of the Loughborough Antennas and Propagation Conference Best Paper Award in 2007, the Best Poster Award in the field of metamaterial applications in antennas at the Metamaterials Conference in 2009, the Excellence Award to Young Research Staff at the University Carlos III of Madrid in 2014, and the Third Place Winner of the Bell Labs Prize in 2014. She is an Associate Editor of the *IEEE Antennas and Propagation Magazine* and the *IEEE Antennas and Wireless Propagation Letters*.

Antonio Montesano Benito was born in Madrid, Spain, in 1964. He received the Degree in telecommunication engineering from the Polytechnic University of Madrid, Madrid, in 1988, with a specialization in communications, microwaves, antennas, and electromagnetic field.

He started his professional career activity in early 1988, as a young graduate, with the Space Division, CASA, Madrid, participating in several reflector and array antenna design and testing in Ku-, Ka-, C-, and L-band as a Design and Test Engineer, mainly for space segment applications, such as deep space, navigation, earth observation, science, or telecommunications, with the development of the necessary technologies for the implementation for such exigent environments. In parallel, he was responsible for the company RF and antenna test facility setup in the Madrid Barajas site in 1991, and its operation till 1999. Responsible for RF designs, technical coordination, and R&D projects, he is the Head of the Array Antenna Section with EADS CASA Espacio, Madrid (AIRBUS Defence and Space, Spain). He has participated in emblematic projects, such as the DBS antenna of HISPSAT 1A y 1B (first Space deployable reflector developed in Spain), the antennas of the advanced synthetic aperture RADAR of ENVISAT for ESA, the LARSAR, or the PAZ; the navigations antenna of IMARSAT and GALILEO; and scientific missions like the HGA of MARS EXPRESS and VENUS EXPRESS, MGA of ROSETA, all those for ESA and the HGA of the Mars Science Laboratory of the CURIOSITY that for NASA. In the field of the active antennas, he has participated in the development of mutibeam steerable and reconfigurable antennas for telecom, such as In-orbit Reconfigurable Multibeam Antenna for telecom in X-band, part of SPAINSAT from HISDESAT, or ELectronically eStirable Antenna (ELSA) for telecom in Ku-band, part of HISPASAT AG, and currently of ELSA+ for EUTELSAT QUANTUM satellite in Ku-band; or single beam steerable semiactive antenna of GAIA telescope in X-band. He has authored several articles in congress related with the developed projects, and participated in the book entitled *Space Antenna Handbook* (Wiley, 2012). He was part of the Multipaction Working Group during the multination standard definition, and coordinated high power, PIM corona, and multination test activities with ESTEC, INTA, and DFL.

Nuria Llombart (S'06–M'07–SM'13) received the Electrical Engineering and Ph.D. degrees from the Polytechnic University of Valencia, Valencia, Spain, in 2002 and 2006, respectively.

She spent one year with the Friedrich-Alexander University of Erlangen–Nuremberg, Erlangen, Germany, and the Fraunhofer Institute for Integrated Circuits, Erlangen, during her master's studies. From 2002 to 2007, she was with the Antenna Group, TNO Defence, Security and Safety Institute, The Hague, The Netherlands, as a Ph.D. Student and then a Researcher. From 2007 to 2010, she was a Post-Doctoral Fellow with the Submillimeter Wave Advance Technology Group, Jet Propulsion Laboratory, California Institute of Technology, Pasadena, CA, USA. She was a Ramn y Cajal Fellow with the Optics Department, Complutense University of Madrid, Madrid, Spain, from 2010 to 2012. In 2012, she joined the THz Sensing Group, Delft University of Technology, Delft, The Netherlands, where she is currently an Associate Professor. She has co-authored over 150 journal and international conference contributions. Her current research interests include the analysis and design of planar antennas, periodic structures, reflector antennas, lens antennas, and waveguide structures, with an emphasis on the THz range.

Dr. Llombart was a co-recipient of the H. A. Wheeler Award for the Best Applications Paper of the Year 2008 in the IEEE TRANSACTIONS ON ANTENNAS AND PROPAGATION, the 2014 THz Science and Technology Best Paper Award of the IEEE Microwave Theory and Techniques Society, and several NASA awards. She received the 2014 IEEE Antenna and Propagation Society Lot Shafai Mid-Career Distinguished Achievement Award. In 2015, she also received a European Research Council Starting Grant. She serves as a Board Member of the IRMMW-THz International Society and a Topical Editor of the IEEE TRANSACTIONS ON THZ SCIENCE AND TECHNOLOGY and the *IEEE Antennas and Propagation Wireless Letters*.